

Complete Valorisation of Lignocellulose and Low Concentration CO₂ using a Fractionation-Photocatalysis-Electrolysis Process

Santiago Rodríguez-Jiménez^{1,2}, Erwin Lam^{1,2}, Subhajit Bhattacharjee¹, Erwin Reisner^{1*}

¹Yusuf Hamied Department of Chemistry, University of Cambridge, Lensfield Road, CB2 1EW, Cambridge, UK.

²These authors contributed equally.

*Corresponding author. E-mail: reisner@ch.cam.ac.uk

Abstract

The simultaneous upcycling of all components in lignocellulosic biomass and the greenhouse gas CO₂ presents an attractive opportunity to synthesise sustainable and valuable chemicals. However, this approach has not yet been realised, presumably due to the difficulty of implementing a solution process to convert a robust and complex solid (lignocellulose) with a barely soluble and stable gas (CO₂). Herein, we present the complete oxidative valorisation of lignocellulose coupled to the reduction of low concentration CO₂ through a three-step fractionation-photocatalysis-electrolysis process. Lignocellulose from white birch wood was first pre-treated using an acidic dioxane solution to generate predominantly cellulosic- and lignin-based fractions. The solid cellulosic-based fraction was solubilised using cellulase (a cellulose depolymerising enzyme), followed by photocatalytic oxidation to formate with concomitant reduction of CO₂ to syngas (a gas mixture of CO and H₂) using a phosphonate-containing cobalt(II) bis(terpyridine) catalyst immobilised onto TiO₂ nanoparticles. Photocatalysis generated 27.9±2.0 μmol_{CO} g_{TiO₂}⁻¹ (TON_{CO} = 2.8±0.2; 16% CO selectivity) and 147.7±12.0 μmol_{formate} g_{TiO₂}⁻¹ after 24 h solar light irradiation under 20 vol% CO₂ in N₂. The soluble lignin-based fraction was oxidised in an electrolyser to the value-added chemicals vanillin (0.62 g kg_{lignin}⁻¹) and syringaldehyde (1.65 g kg_{lignin}⁻¹) at the anode, while diluted CO₂ (20 vol%) was converted to CO (20.5±0.2 μmol_{CO} cm⁻² in 4 h) at a Co(II) porphyrin catalyst modified cathode (TON_{CO} = 707±7; 78% CO selectivity) at an applied voltage of 3 V. We thus demonstrate the complete valorisation of solid and a gaseous waste stream in a liquid phase process by combining fractioning, photo- and electrocatalysis based on earth-abundant molecular hybrid nanomaterials.

Introduction

The renewable generation of valuable chemicals and fuels is a critical step towards a sustainable and circular life cycle of chemicals.^{1, 2} The valorisation of abundant waste resources, such as lignocellulosic biomass and the greenhouse gas CO₂ offers great potential to achieve such an ambitious goal. By harnessing the power of renewable energy sources, such as solar and wind, the conversion of non-edible biomass and CO₂ via photo- or electrochemical approaches presents an opportunity to produce sustainable fuels and chemicals.³

Lignocellulosic biomass such as wood, is abundant and cheap and consists predominantly of three polymeric components: cellulose, hemicellulose and lignin.^{4, 5} Cellulose and hemicellulose consist mainly of polysaccharose made from glucose, xylose, mannose and arabinose. Lignin is made of different polymerised aromatic units, and its utilisation remains challenging due to the robustness of its polyaromatic structure, which requires harsh conditions to break down the polymer (e.g., strong acids such as H₂SO₄).^{6, 7} Unlike cellulose, lignin-to-chemical conversion technologies remain scarce.^{4, 5, 7, 8} An important linkage in lignin, often found between its aromatic polymeric backbone, is the β-O-4 bond between two phenyl rings, which serves as an ideal target to depolymerise lignin into smaller fragments.⁹⁻¹¹ Thus, the selective depolymerisation of all lignocellulose components and their subsequent chemical transformation would enable large-scale access to aliphatic and aromatic renewable feedstock chemicals.

Apart from ubiquitous biomass sources, the greenhouse gas CO₂ can be used as an abundant carbon source to produce energy-rich chemicals such as CO, formate, hydrocarbons or alcohols.¹² However, photo- and electroreduction of CO₂ are predominantly performed in the presence of pure CO₂, where concentrated CO₂ streams have to be generated involving additional energy input.¹³⁻¹⁵ To alleviate the energy demand of the process, it is desirable to perform catalytic reactions at lower CO₂ concentrations (e.g., ≤ 20% CO₂).¹⁶⁻²⁰ The challenge of using low concentration CO₂ streams lies in maintaining high product selectivity and catalytic activity compared to reactions employing pure CO₂ streams.¹⁷ Molecular CO₂ reduction catalysts display an increased product selectivity compared to most heterogenous electro- or photocatalysts.^{16, 21, 22}

An attractive approach to utilise biomass and CO₂ together is their simultaneous conversion in photo- or electrocatalytic processes.²³⁻²⁵ This strategy opens the possibility to couple biomass oxidation with CO₂ reduction in a single process driven by sunlight or renewable electricity. The coupling of productive half-reactions thereby allows the conversion of a solid and a gaseous waste stream into valuable products such as CO, syngas, formate and

aromatic chemicals, which can be more attractive than conventional systems performing overall water splitting to generate H₂ and O₂ from water. Additionally, the oxidation of biomass-derived substrates is thermodynamically less demanding than water oxidation, thereby facilitating the catalytic conversions, as well as the generation of added value products.²⁶⁻²⁸ This combined approach also allows for the isolation of products in different phases and compartments, which can help with product separation. Conventional approaches such as water splitting generate explosive H₂ and O₂ mixtures in the reactor headspace.

The valorisation of cellulose and CO₂ streams has recently been reported using a TiO₂ nanoparticle with an immobilised CO₂ reducing cobalt(II) bis(terpyridine) catalyst containing phosphonate anchors (**CotpyP**) (TiO₂|**CotpyP**). Photoexcitation of this hybrid TiO₂|**CotpyP** photocatalyst reduced aqueous CO₂ to syngas, while cellulose-derived glucose was simultaneously oxidised to formate and arabinose. TiO₂|**CotpyP** could operate for 24 h and be recycled up to three times.²⁹ However, only concentrated CO₂ and pure cellulose have been used, and no strategy for lignin separation and utilisation were reported in this previous study.

Herein, we report the first example of complete lignocellulose valorisation coupled to low concentration CO₂ reduction, which has been achieved by employing selective molecular CO₂ reduction hybrid nanomaterials (Figure 1). First, lignocellulose is pre-treated and fractionated into predominantly cellulosic- and lignin-based components using acid hydrolysis and solubilisation. Second, the fractionated cellulosic solution was converted with low concentration CO₂ using the TiO₂|**CotpyP** photocatalyst to HCOO⁻ and syngas, respectively. Finally, an electrolysis process concomitantly converted the fractionated lignin solution on a carbon-based anode to vanillin and syringaldehyde, which find application in the food, pharma and cosmetics industries.^{10, 30} Diluted CO₂ is reduced to CO (with a single pass conversion efficiency close to 5% at both 10vol% and 20vol% CO₂) with a molecular cobalt(II) porphyrin (**CoP_L**) catalyst immobilised on a multiwall carbon nanotube (MWCNT) cathode. Thus, we demonstrate the complete valorisation of lignocellulose and low concentration CO₂, which has been enabled by a precious-metal free fractionation-photocatalysis-electrolysis process.

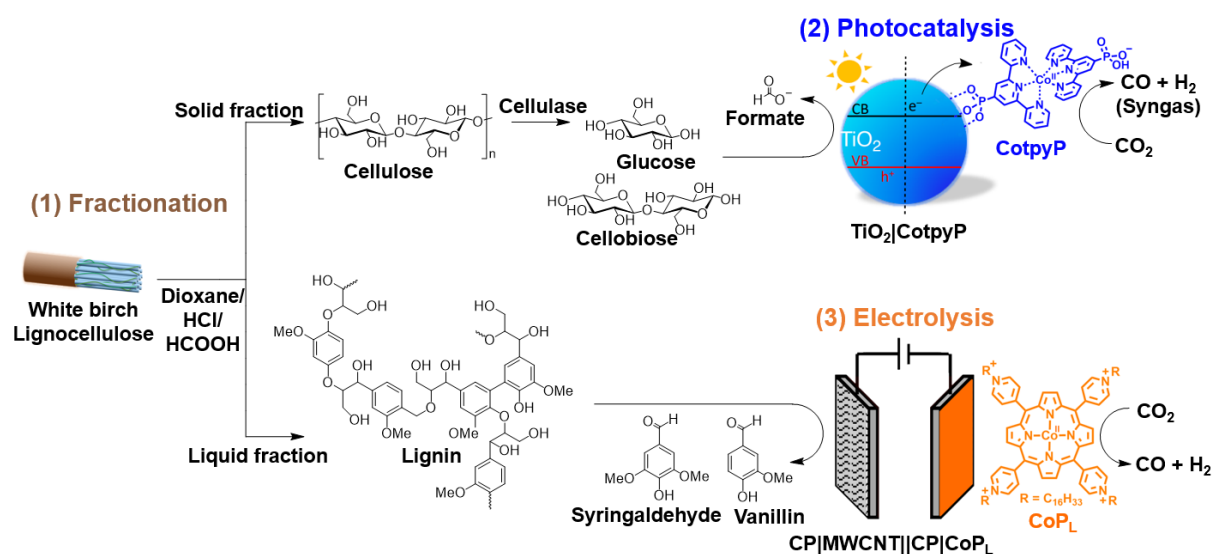


Figure 1. Three-step process: (1) fractionation, (2) photocatalysis and (3) electrolysis. Schematic overview of a three-stage process for complete valorisation of lignocellulose and diluted CO₂. (1) Fractionation of lignocellulose from white birch into a predominant cellulose and lignin fraction (top and bottom, respectively), with the cellulose-based solid fraction being further incubated in cellulase to generate a soluble sugar (glucose and cellobiose) solution. Structures of xylose, mannose and arabinose are omitted for clarity. (2) Photocatalytic oxidation of cellulose-derived glucose and cellobiose to formate coupled with reduction of diluted CO₂ to syngas (CO and H₂) using TiO₂|**Coptyp** photocatalyst. (3) Electrolytic oxidation of lignin to aromatic aldehydes syringaldehyde and vanillin coupled with reduction of diluted CO₂ to CO and H₂ using CP|MWCNT||CP|CoP_L.

Results and Discussion

Fractionation of Lignocellulose

The composition of dried and extracted white birch wood used in this study was determined by quantifying its sugar and lignin composition following standard procedures using H₂SO₄ hydrolysis:⁶ glucose (34.7±1.6 wt%), xylose (20.3±1.0 wt%), mannose (1.8±0.1 wt%), arabinose (0.9±0.1 wt%) and lignin (17.6±1.4 wt%). Further details are provided in the Experimental Section, Figure 1, Figure S1 and Tables S1 and S2.

To effectively utilise the different components of lignocellulose, their individual components are first separated by acid hydrolysis and solubilisation. Lignocellulose was pre-treated in a dioxane/HCl/HCOOH mixture at 80 °C for 3 h (500 mg in 5.9 mL) to obtain a liquid (or liquor) and a solid fraction.⁷ The dioxane/HCl/HCOOH mixture solubilises lignin and the liquid fraction predominantly consisted of lignin (41.2±2.1 wt%) along with xylose (6.9±1.3 wt%), glucose

(2.4±0.6 wt%), mannose (1.3±0.3 wt%) and arabinose (2.5±0.7 wt%). The second most abundant component xylose (derived from hemicellulose) is partially converted to furfural under these fractioning conditions (see experimental Section, and Figure 1, Figure S1 and Tables S1-S3 for further details).²⁶ The isolated solid fraction consisted mainly of cellulosic components such as glucose (62.9±1.9 wt%) and xylose (6.7±1.6 wt%) with some lignin (5.4±1.2 wt%).

Photocatalytic Valorisation of Cellulose and CO₂

The solid fraction obtained from lignocellulose fractionation contained mainly cellulose and was used as a feedstock in photocatalysis following depolymerisation via cellulase pre-treatment.²⁹ The depolymerised glucose and cellobiose are suitable electron donors in semiconductor suspension systems,³¹ and their valorisation has been previously reported.^{32, 33} Specifically, the solid fraction was enzyme pre-treated with cellulase (0.05 mg_{cellulase} mg_{solid}⁻¹) to generate soluble sugars, predominantly glucose (39.3±4.7 mM) and cellobiose (8.7±2.1 mM) after 24 h incubation at 37 °C in an aqueous sodium acetate buffer solution (50 mM) at pH 5.²⁹ With respect to white birch, 10.2±0.4 wt% and 4.2±0.6 wt% were converted to glucose and cellobiose, respectively (see Tables S1 and S2).

The lignocellulose-derived sugar solution was then utilised for CO₂ reduction reactions using the TiO₂|**CotpyP** photocatalyst (Figure 1).²⁹ In a typical experiment, **CotpyP** (50 nmol) was added to a photoreactor containing a TiO₂ suspension (5 mg, P25, particle diameter ~20 nm) in 2:1 MeCN:enzyme-treated solid fraction aqueous solution (3 mL). The photoreactor was sealed with a rubber septum and purged with 100% CO₂ or 20% CO₂ (balanced with N₂) at a flow rate of 15 mL min⁻¹ for 15 min. The sealed and stirred photoreactor was irradiated with a solar light simulator (100 mW cm⁻², AM 1.5G, 25 °C, 600 rpm) for 24 h. The UV in the full solar spectrum is necessary to photoexcite electrons from the valence to the conduction band of TiO₂.²⁹ The gaseous products (H₂ and CO) in the headspace (4.74 mL) were quantified by gas chromatography (GC), and HCOO⁻ formed in the solution from glucose photooxidation was quantified by ion chromatography.

After 24 h of photocatalysis under 100 vol% CO₂, 69.9±4.0 μmol_{CO} g_{TiO₂}⁻¹, 109.8±8.0 μmol_{H₂} g_{TiO₂}⁻¹ (i.e., 39% CO and 61% H₂ selectivity for gaseous products) and 153.7±4.0 μmol_{formate} g_{TiO₂}⁻¹ were formed. Under 20 vol% CO₂, the formation yields were 27.9±2.0 μmol_{CO} g_{TiO₂}⁻¹, 141.7±27.9 μmol_{H₂} g_{TiO₂}⁻¹ (i.e., 16% CO and 84% H₂ selectivities) and 147.7±12.0 μmol_{formate} g_{TiO₂}⁻¹ (Figure 2a and Table S4). The obtained CO yields correspond to a CO₂-to-CO conversion efficiencies of ~0.03% and ~0.05% at 100vol% and 20vol% CO₂, respectively. The

reduction of protons (from water) to H_2 ³⁴ and CO_2 to CO ³⁵ as well as the oxidation of glucose/cellobiose to formate are two-electron processes with an expected 1:1 stoichiometric ratio for (H_2+CO) :formate,²⁹ which is close to the observed ratios.

The carbon source of the products was confirmed by isotopic labelling experiments. Experiments with $^{13}\text{CO}_2$ and cellulase enzyme pre-treated cellulose were performed to confirm that the CO originates from CO_2 reduction (for further details see Experimental section). Analysis of the gas headspace after photocatalysis by transmission IR spectroscopy reveals that ^{13}CO produced by TiO_2 |**CotpyP** was only formed when $^{13}\text{CO}_2$ was used as the carbon source (Figure 2b). Furthermore, in the case of formate, based on previous work using $^{13}\text{C}_6$ -glucose with TiO_2 |**CotpyP**, ^{13}C -formate is only formed from photooxidation of $^{13}\text{C}_6$ -glucose, confirming formate's carbon source.²⁹

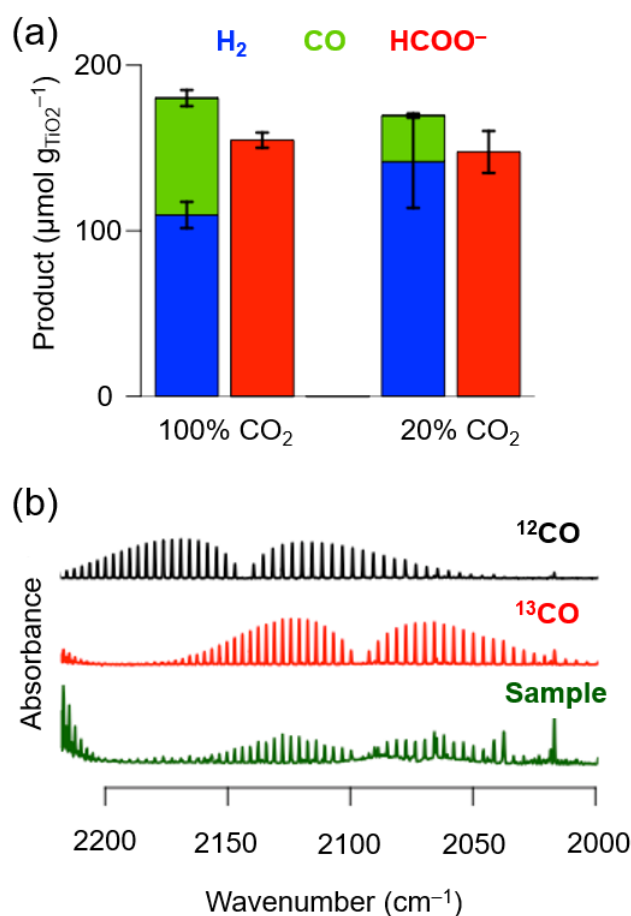


Figure 2. (a) H_2 , CO and formate (blue, green and red, respectively) formation after 24 h of photocatalysis with TiO_2 |**CotpyP**. (b) Transmission IR spectra with $^{13}\text{CO}_2$ isotopic labelling of the headspace after 24 h of photocatalysis (sample, green curve), including ^{12}CO (black) and ^{13}CO (red) as reference. Reaction conditions: 5 mg TiO_2 (P25); 50 nmol **CotpyP**; 3 mL 2:1 MeCN:pre-treated reaction solution (cellulose fraction pre-treated with cellulase); 25 °C, 100

mW cm⁻², AM 1.5G. (a) 20 vol% CO₂ was balanced with N₂; (b) sample (green) was purged with 100% ¹³CO₂. Experiments in Figure 2a were performed in triplicates.

These results demonstrate that the cellulose solid fraction, following cellulase pre-treatment, provides a source of suitable electron donors for photocatalytic CO₂ reduction. The solar TiO₂|**CotpyP** reforming system was able to convert CO₂-to-CO at concentrations of 20 vol% CO₂, with an activity drop of only a factor of two despite the five-fold drop in CO₂ concentration with respect to 100 vol% CO₂ (Figure 2a). Near stoichiometric amounts of HCOO⁻ to CO/H₂ were formed at both CO₂ concentrations, demonstrating the effectiveness of TiO₂|**CotpyP** to photooxidise sugars to formate and concomitantly photoreduce CO₂ and H₂O to CO and H₂.

Electrolytic Valorisation of Lignin and CO₂

To optimise the simultaneous electrolysis of CO₂ and lignin, the half-reactions of electroreduction of low CO₂ concentration and electrooxidation of lignocellulose-derived lignin were first studied individually in a three-electrode setup. This was followed by the proof-of-concept coupling of both half reactions in a two-electrode electrolyser using the optimised cathode and anode.

Low concentration CO₂ electroreduction was performed on **CoP_L** immobilised on MWCNT as a molecular catalyst (see Figure 1). **CoP_L** was chosen based on its known CO selectivity during electroreduction of pure CO₂, and stability when immobilised on MWCNT via π-π stacking and its lipophilic alkyl chains (see Supplementary Note 1, and Figures S2-S4).^{28, 36} We therefore further explored the electroreduction ability of **CoP_L** supported on MWCNT under variable CO₂ concentrations ranging 10, 20, 50 and 100 vol% (balanced with N₂), using an electrochemical flow setup that allowed continuous purging of the electrolyte solution with a given gas composition.³⁷

Cathodes containing **CoP_L** were prepared, following a reported procedure (see Figure S5),²⁸ by drop-casting a dimethylformamide (DMF) suspension containing 2.37 mg MWCNT mL⁻¹ and 0.1 mM **CoP_L** onto carbon paper (CP) (0.1 mL_{DMF} cm⁻², geometrical surface area = 1 cm²), which is denoted as CP|**CoP_L**. Electrocatalysis with CP|**CoP_L** was performed in a two-compartment electrochemical cell with a three-electrode setup. Pt foil was used as counter electrode (CE) and Ag/AgCl (sat. KCl) as reference electrode (RE), a Nafion membrane separating the cathode and anode chambers, with the catholyte (0.1 M NaHCO₃ in H₂O) under a constant gas flow (9 mL min⁻¹) of CO₂ and N₂ regulated by mass flow controllers. The

generated gaseous products during electrochemical experiments (H_2 and CO) were measured via online GC (schematically represented in Figure S6).³⁷

During chronoamperometry (CA) experiments, under an applied potential of -1.2 V vs. Ag/AgCl (sat. KCl) the catholyte chamber was continuously purged with pure N_2 for 30 min, after which the CO_2 concentration was gradually increased to 10, 20, 50 and 100 vol% every 45 min (Figure 3a). Under pure N_2 , the current density was the lowest at approximately -0.5 mA cm^{-2} and around ~ 0.08 $\mu\text{mol}_{\text{H}_2} \text{min}^{-1}$ evolved as the main gaseous product, with a minor CO background (< 0.01 $\mu\text{mol}_{\text{CO}} \text{min}^{-1}$) likely caused by the chemical equilibrium between carbonic acid (H_2CO_3) and CO_2 . Upon increasing the CO_2 concentration (in vol%), the current density gradually increased, from approximately -0.8 mA cm^{-2} (10 vol%), to -1.2 mA cm^{-2} (20 vol%), to -1.5 mA cm^{-2} (50 vol%) and to -1.8 mA cm^{-2} (100 vol%). The H_2 formation rate remained constant at ~ 0.06 $\mu\text{mol}_{\text{H}_2} \text{min}^{-1}$ at all CO_2 concentration steps, whereas the CO formation rate and CO selectivity increased from ~ 0.12 $\mu\text{mol}_{\text{CO}} \text{min}^{-1}$ and $\sim 65\%$ (10 vol%), to ~ 0.24 $\mu\text{mol}_{\text{CO}} \text{min}^{-1}$ and $\sim 80\%$ (20 vol%), to ~ 0.35 $\mu\text{mol}_{\text{CO}} \text{min}^{-1}$ and $\sim 90\%$ (50 vol%) and to ~ 0.50 $\mu\text{mol}_{\text{CO}} \text{min}^{-1}$ and $\sim 93\%$ (Figure 3b). The H_2 formation rate across all studied CO_2 concentrations may be explained by the high affinity of **CoP_L** to CO_2 .²⁸

Two main observations can be made by screening different CO_2 gas flow concentrations: (1) **CoP_L** exhibits a high product specificity with around $\sim 80\%$ CO selectivity even under 20 vol% of substrate CO_2 . (2) The CO formation rate at 20 vol% CO_2 (~ 0.24 $\mu\text{mol}_{\text{CO}} \text{min}^{-1}$; CO turnover frequency (TOF_{CO}) = 8.3 min^{-1} ; single-pass CO_2 conversion efficiency³⁸ (SPCCE) = 4.7%) corresponds to roughly half the activity with respect to 100 vol% CO_2 (~ 0.50 $\mu\text{mol}_{\text{CO}} \text{min}^{-1}$; TOF_{CO} = 17.2 min^{-1} ; SPCCE = 2.0%), thus indicating that decreasing five-fold the CO_2 concentration only reduces two-fold the CO formation rate (Figure 3b). Si

When comparing $\text{CP}|\text{CoP}_{\text{L}}$ with $\text{TiO}_2|\text{CotpyP}$, both molecular systems exhibit similar CO formation rate trends, although $\text{CP}|\text{CoP}_{\text{L}}$ maintains higher CO selectivity across all CO_2 concentrations (see Supplementary Note 1 and Tables S4 and S5). The origin of the observed trends for $\text{TiO}_2|\text{CotpyP}$ and $\text{CP}|\text{CoP}_{\text{L}}$ at different CO_2 concentrations remains unclear but may be attributed to their molecular structure, which provides intrinsic affinity towards CO_2 . In comparison with state-of-the-art molecular systems, such as the rhenium bipyridine electrocatalyst $[\text{Re}(4,4\text{-dimethyl-2,2-dipyridyl})(\text{CO})_3(\text{triethanolamine})]$, which operates in a $\text{DMF}/\text{triethanolamine}$ solvent mixture at variable CO_2 concentrations (1, 10 and 100 %) under comparable flow conditions,²² $\text{CP}|\text{CoP}_{\text{L}}$ is three orders of magnitude more active (i.e., TOF_{CO} = 0.5 h^{-1} after 24h at 10% CO_2 vs 413 h^{-1} after 4h at 20% CO_2 , respectively). Without taking into account that CO_2 is more soluble in organic solvents than in water (e.g. ~ 180 mM in DMF vs ~ 33 mM in water at 25 °C), these differences in performance could be tentatively associated

to the catalytic mechanism of CO₂ reduction, which enables cobalt porphyrins to achieve higher TOF than rhenium bipyridine electrocatalysts.^{22, 36}

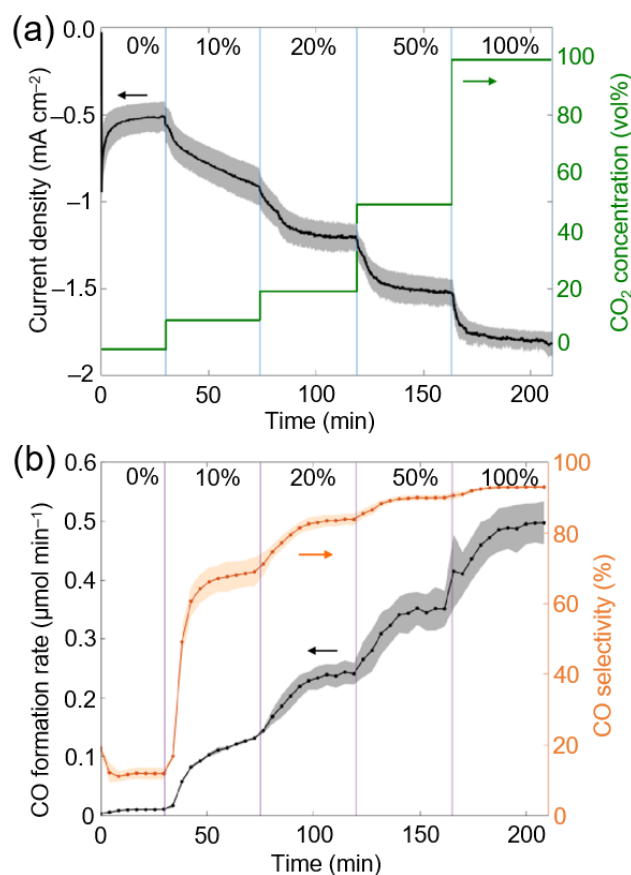


Figure 3. (a) Chronoamperometry (CA) experiments as a function of concentration of CO₂ and time during CO₂ electrochemical reduction to CO using CP|CoP_L cathodes. (b) CO formation rate and selectivity during CA experiments. Experiments were performed in triplicates, and the shaded area represents the standard error. Reaction conditions: CA: 0.1 M NaHCO₃ in H₂O (pH = 6.7); E_{app} = -1.2 V vs. Ag/AgCl for 3.5 h; WE: CP|CoP_L, CE: Pt foil, RE: Ag/AgCl (sat. KCl). Flow of CO₂:N₂ 9 mL min⁻¹. CO₂ concentration was varied stepwise between 0 vol%, 10 vol%, 20 vol%, 50 vol% and 100 vol% and balanced with N₂.

The electrooxidation of the liquid fraction or liquor, containing predominantly lignin and obtained from pre-treating lignocellulose (250 mg), was studied in a two-compartment electrochemical cell with a three-electrode setup. For this purpose, the anodic conditions were initially optimised using the lignin model substrate 1-(3,4-dimethoxyphenyl)-2-(2-methoxyphenoxy)propane-1,3-diol, which contains a β-O-4 linkage between two phenyl rings that mimics those ubiquitously found in lignin (see Figure 1 and Figure S7).⁹⁻¹¹

CP|MWCNT anodes were fabricated by dropcasting a MWCNT suspension in ethanol (1.67 mg mL^{-1} , 0.1 mL cm^{-2}) containing Nafion 117 (2 vol% of a 5 wt% solution) to achieve a high surface area MWCNT layer with $\sim 200 \text{ }\mu\text{m}$ thickness (see Figure S8). We found that MWCNT on hydrophilic carbon paper (CP|MWCNT) acted as a suitable catalyst for the oxidation of the β -O-4 linkage in the model substrate (see Figure S7 and Supplementary Note 2). CP|MWCNT (geometric surface area = 1 cm^2) in the presence of 10 mM of lignin model substrate in 0.1 M Na_2CO_3 in 1:1 MeCN:H₂O achieved high current densities ($\sim 8 \text{ mA cm}^{-2}$) at +1 V vs Ag/AgCl (sat. KCl), while in absence of lignin, and under the same conditions, the current densities were lower ($\sim 3 \text{ mA cm}^{-2}$) (see Figures S9 and S10). MeCN was used to increase the solubility of the lignin model substrate and lignin; and the lower current observed in the absence of lignin may be ascribed to water oxidation. The generated oxidation product from the lignin model substrate during CA experiments, 3,4-dimethoxybenzaldehyde (3,4-MBA), was obtained in $35.6 \pm 1.1\%$ yield with a Faradaic yield (FY) of $24.9 \pm 0.7\%$ assuming a two-electron oxidation (see Experimental details, Figure S11 and Table S6). The obtained 3,4-dimethoxybenzaldehyde was measured by ^1H nuclear magnetic resonance (NMR) in CDCl_3 with mesitylene as internal standard (see Figures S12-S14).

Having established the optimised conditions (see Supplementary Note 3, and Figures S15-S20) and the electrodes suitable for lignin oxidation and low concentration CO_2 reduction, we aimed at coupling both redox half reactions in a single two-electrode electrolyser with the corresponding anolytes and catholytes separated by a bipolar membrane. Electrolysis was performed using a two-electrode setup (CP|CoP_L as WE and CP|MWCNT as CE) with an applied voltage (U_{app}) of +3 V for 4 h. The anolyte comprised of 0.1 M Na_2CO_3 in a 1:1 MeCN:H₂O solvent mix containing lignin (obtained from pre-treating 250 mg lignocellulose), and the catholyte had 0.1 M NaHCO_3 in H₂O. The catholyte was constantly purged at 9 mL min^{-1} with 20 vol% CO_2 (balanced with N_2). The gaseous products on the cathodic side were monitored by online GC.³⁷

During 4 h electrolysis, the initial current density gradually decreased from approximately -1.4 mA cm^{-2} to around -0.4 mA cm^{-2} (Figure S21), and the initial maximum CO formation rate observed changed from $\sim 0.2 \text{ }\mu\text{mol}_{\text{CO}} \text{ min}^{-1}$ to $\sim 0.05 \text{ }\mu\text{mol}_{\text{CO}} \text{ min}^{-1}$ (Figures 4a and 4b). After 4 h, $20.5 \pm 0.2 \text{ }\mu\text{mol}_{\text{CO}} \text{ cm}^{-2}$ was produced along with $5.8 \pm 0.3 \text{ }\mu\text{mol}_{\text{H}_2} \text{ cm}^{-2}$ ($\text{TON}_{\text{CO}} = 707 \pm 7$ and $\text{TON}_{\text{H}_2} = 200 \pm 10$) corresponding to a CO selectivity of $77.8 \pm 2.0\%$ and a $\text{FY}_{\text{CO}+\text{H}_2}$ of $59.0 \pm 5.5\%$ (Table S5). Despite of the decrease in current density and CO formation rates, the CO selectivity remained stable, highlighting the structural stability of CoP_L.²⁸

After electrolysis, the anolyte was worked-up (see Experimental Section for details) and the crude product was analysed by ^1H NMR in CDCl_3 . Control experiments, where the lignin

fraction was stirred in the electrolyte solution for 4 h without applied bias, led to the formation of a small background level of aldehydes. Importantly, under an applied potential more aromatic aldehydes signals were formed (Figures S20 and 4c), which shows that aromatic monomer formation is promoted by electrooxidation. The observed ^1H NMR signals corresponded to syringaldehyde and vanillin (see Figure 1, and Figure 4c), which are aromatics that can be formed from lignin.^{8, 10} After 4 h CA, $0.14\pm 0.03\ \mu\text{mol}$ and $0.31\pm 0.03\ \mu\text{mol}$ of vanillin and syringaldehyde were detected, respectively. These yields equated to 0.62 g of vanillin and 1.65 g of syringaldehyde per kilogram of lignin. Compared with oxygen evolved from water oxidation, vanillin and syringaldehyde have potential as bio-derived monomers in the polymer industry.³⁹ The observed moderate yields for vanillin and syringaldehyde could be attributed to the acidic degradation of reaction intermediates, i.e., lignin-fragment oxidation decreased the local pH at the CP|MWCNT anode surface below 11.5, and hence halt the formation of the targeted aromatics.³⁹ In addition to the two identified aromatic compounds, other unidentified signals in the aromatic aldehyde (~ 9.8 ppm) and methoxy regions (3.8-4.0 ppm) can be observed in the ^1H NMR spectra (Figure 4c).³⁹

In comparison with CP|MWCNT, the use of heterogeneous anodes for lignin oxidation based on metals/metal oxides, such as toxic Pb/PbO₂, has been reported.⁴⁰⁻⁴² For instance, these Pb/PbO₂ anodes were able to generate different lignin-derived products, such as vanillin (5.83 g kg_{lignin}⁻¹) and syringaldehyde (9.30 g kg_{lignin}⁻¹), via electrooxidation/electrohydrogenation of bamboo-derived lignin when used with Cu cathodes in 1 M NaOH solution.⁴⁰ Despite the difficulty to compare this previously reported system with our CP|MWCNT||CP|CoP_L system due to the different experimental conditions (i.e., electrode materials and surface, pH, temperature, substrate concentration, applied voltage and currents), the metal-free CP|MWCNT anodes were able to generate yields of vanillin and syringaldehyde within the same order or one-order of magnitude lower than those reported for the metal/metal oxide based Pb/PbO₂||Cu system.

Previous work has shown that lignin valorisation can be coupled with hydrogen evolution or reduction of CO₂ to formate using photoelectrochemical systems.^{43, 44} In comparison, our work presents a unique and successful three-step approach that shows that complete valorisation of lignocellulose is possible through the combination of fractionation and utilisation of photocatalysis and electrocatalysis to oxidise the resulting solid fraction to formate and liquid fraction to aromatics and reduce diluted CO₂ and water to CO and H₂. Although this system is a proof-of-concept demonstration, different factors would need consideration for practical implementation. These include scalability,^{45, 46} integration of a carbon capture step,⁴⁷ potential limitations such as catalyst stability, the engineering design of reactors^{48, 49} for lignocellulose

fractionation,⁴⁵ photocatalysis⁵⁰ and electrolysis,⁵¹ and the separation of products for further use.^{52, 53}

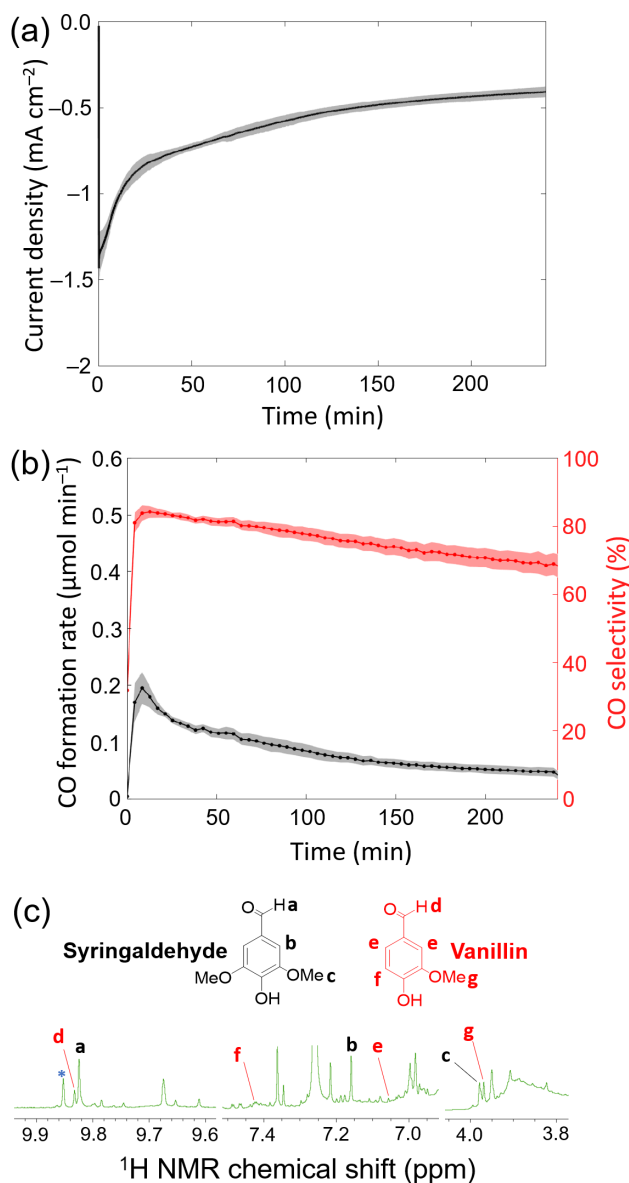


Figure 4. CO₂ electroreduction under 20 vol% CO₂ gas flow with CP|CoP_L coupled to lignin conversion at the anode with CP|MWCNT. (a) Current density as a function of time. (b) CO formation rate and selectivity during electrolysis. (c) ¹H NMR in CDCl₃ of the anolyte containing lignin after 4 h electrocatalysis showing the emergence of aldehydes and methoxy groups. Experiments were performed in triplicates, and standard errors are represented as shaded area (a, b). Reaction conditions: (a and b) Electrolysis at U_{app} = +3 V. Anolyte: 0.1 M Na₂CO₃, lignin fraction obtained from pre-treating 250 mg Lignocellulose in 1:1 MeCN:H₂O; Anode: CP|MWCNT. Catholyte: 0.1 M NaHCO₃ in H₂O Flow of 20 vol% CO₂ (balanced with N₂) 9 mL min⁻¹; Cathode: CP|CoP_L; room temperature. (c) The asterisk (*) highlights the additional aldehyde signal formed from lignin electrooxidation.

Conclusions

We report a combined fractionation-photocatalysis-electrolysis process for the complete valorisation of lignocellulose and low-concentration CO₂. Fractioning lignocellulosic wood provides sugar-based solid and lignin-based soluble fractions that are photo- and electrocatalytically converted with immobilised molecular cobalt(II) catalysts to produce CO, formate, vanillin and syringaldehyde. The presented results set a new milestone in integrated renewable processes for complete waste feedstock valorisation under ambient pressure and temperature. Moreover, our molecular hybrid systems were able to convert low CO₂ concentrations (10-20vol% CO₂), which paves the way towards utilising CO₂ concentrations nearing those found in flue gas (4-10vol% CO₂). However, to utilise actual flue gas additional CO₂ purification steps are necessary to eliminate impurities,⁵⁴ such as SO₂, SO₃, NO_x, O₂ and particulate matter depending on the type of fuel used.

Hence, this work demonstrates a new proof-of-concept strategy to valorise challenging multicomponent waste streams simultaneously through solar-driven and electrochemical redox processes. This work further highlights the potential of molecular hybrid systems in the valorisation of waste streams, which can be expanded beyond CO₂ reduction in future developments to perform chemistry in a more sustainable and circular manner.

Experimental Section

Solvents and materials. Acetonitrile (MeCN, Fisher Chemicals), D₂O (Sigma Aldrich), D(+)-glucose (Fisher Chemicals), D(+)-cellobiose (Acros), Cellulase from *Trichoderma reesei* ATCC 26921 (Sigma Aldrich), sodium acetate trihydrate (Fisher Chemicals), hydrochloric acid (34-37% Fisher Chemicals) 1-(3,4-dimethoxyphenyl)-2-(2-methoxyphenoxy)propane-1,3-diol (lignin model substrate, FluoroChem), Vanillin (Thermo Scientific), syringaldehyde (Thermo Scientific), vanillic acid (Sigma Aldrich), syringic acid (Thermo Scientific), fufural (Sigma Aldrich), 2-methoxyphenoxyacetic acid (Alfa Aesar), 3,4-dimethoxybenzaldehyde (Acros) 4-hydroxybenzoic acid (Thermo Scientific), white birch (Merck), dioxane (Fisher Chemicals), formic acid (Fisher Chemicals), sulfuric acid (Fisher Chemicals), multiwalled carbon nanotubes (MWCNT 755117, Sigma Aldrich), carbon paper (Toray Paper 60, Fuel Cell Store), Nafion solution (5 wt% Sigma Aldrich), NaHCO₃ (Merck), EtOAc (Fisher Chemicals), THF (Fisher Chemicals), Na₂CO₃ (Merck), MgSO₄ (Fisher Chemicals) CDCl₃ (Sigma Aldrich), 50wt% H₂SO₄ (Fluka), Na₂CO₃ 64mM and NaHCO₃ 20mM (ion chromatography eluent concentrate for Metrosep A Supp5; Sigma Aldrich) were purchased from commercial sources

and used as received. MilliQ[®] grade H₂O was used for all the experiments. TiO₂ powder P25 (10-30 nm diameter; 50 m² g⁻¹) was obtained from Evonik; [Co(2,2':6',2''-terpyridine-4'-phosphonic acid)₂](BF₄)₂ (denoted as **CotpyP**)³⁵ and **CoP_L**³⁶ were synthesised according to reported procedures. Reaction gases (CO₂ and N₂) were purchased from BOC. Ag/AgCl reference electrode was stored in a saturated NaCl solution (sat. NaCl; BasiMW-2030) and anion exchange membrane (Selemion, AGC Engineering), Nafion 117 membrane (Sigma Aldrich), bipolar membrane (Fumacep, Fuel Cell Store), were stored in MilliQ[®] grade H₂O.

Physical characterisation. ¹H NMR spectroscopy was recorded on a Bruker DPX 400 MHz spectrometer with the chemical shifts (δ) of the ¹H NMR spectrum being referenced against the residual solvent signal (D₂O: δ = 4.79 ppm, CDCl₃: δ = 7.26 ppm). Scanning electron microscopy was performed on a TESCAN MIRA3 FEG-SEM instrument. Before measuring the samples, they were sputtered with 10 nm of platinum.

Product quantification. Gaseous H₂ and CO under static conditions were analysed by an Agilent 7890A gas chromatograph equipped with an HP-5 molecular sieve column and a thermal conductivity detector using He as the carrier gas. The response factors for the gases were determined by calibration with known amounts of H₂ and CO. Typically, 50 μ L of headspace gas from the photoreactor was injected using an air-tight syringe (Hamilton, GASTIGHT). Formate was analysed by ion chromatography (IC) on a Metrohm 882 compact IC plus chromatography system equipped with a Metrosep A Supp 5 – 150/4.0 column using an aqueous Na₂CO₃ (3.2 mM) and NaHCO₃ (1 mM) solution as eluent. The response factor of formate was determined by calibration with known amounts of aqueous formate solutions. Sugar concentrations (Glucose, cellobiose, xylose, mannose and arabinose) were determined by high performance liquid chromatography (HPLC) on a Waters Breeze system equipped with a refractive index detector and a Rezex 8% Ca²⁺ Monosaccharide 300 x 7.80 mm HPLC column using 2.5 mM H₂SO₄ as the eluent with a flow rate of 0.5 mL min⁻¹ (at 75°C). The response factors for the sugars were determined by calibration of aqueous sugar solutions with known amounts of sugar.

Klason lignin and sugar content determination. Klason lignin and sugar determination was performed following a reported procedure.⁶ For the compositional analysis of white birch, the sample was first dried at 105°C overnight followed by cooling to room temperature under static vacuum in a desiccator containing CuSO₄ as drying agent. The dried solid was extracted three times with an ethanol:water mixture (4:1 v/v and 20 mL g⁻¹) followed by water (20 mL g⁻¹) by sonication for 30 minutes. The sample was then dried at 105°C overnight followed by cooling to room temperature under static vacuum in a desiccator containing CuSO₄ as a drying agent.

To determine the Klason lignin content and sugar concentration, to 250 mg of the solid (dried and extracted white birch or solid after white birch pre-treatment in dioxane/HCl/HCOOH) was added 3.75 mL of a 72 wt% H₂SO₄ at room temperature. The suspension was stirred periodically (every 15 min with a glass rod) for 2 h and 145 mL of Milli-Q H₂O was added followed by refluxing the suspension at 120 °C for 4 h. The suspension was filtered on a tared frit. The solid was dried at 105 °C overnight and the mass of the filtered solid was determined gravimetrically to determine Klason Lignin content. The filtrate was diluted with H₂O to 250 mL and concentrated to 50 mL at 80 °C. The solution was then analysed by HPLC to determine the sugar content (glucose, xylose, mannose, galactose and arabinose).

To determine the Klason Lignin and sugar content of the liquor from white Birch pre-treatment in dioxane/HCl/HCOOH, the liquor obtained from pre-treating 500 mg white Birch was used following the same procedure as with dried and extracted white Birch.

White Birch pre-treatment. Lignocellulose fractioning was performed following a reported procedure.⁷ To 500 mg of dried and extracted white birch was added dioxane (4.5 mL), conc. HCl (0.42 mL), formic acid (0.36 mL) and water (0.64 mL). The suspension was then stirred for 5 h at 80 °C and filtered and the residue was washed with dioxane until the solution became clear (solid/cellulose fraction). The combined filtrate was dried at 60 °C under vacuum and extracted with THF followed by drying at 40 °C to obtain a dark oil (liquid/lignin fraction).

Enzyme hydrolysis of pre-treated white Birch. The obtained solid after treatment of white birch with dioxane/HCl/HCOOH was washed three times with H₂O (20 mL g⁻¹) to remove residual HCOOH and dried at 105 °C overnight. To the washed and dried solid fraction (150 mg) in an aqueous sodium acetate solution (50 mM, 3 mL) at pH 5 (adjusted by the addition of HCl) at 37 °C was added cellulase (15 mg in 0.75 mL) in a 50 mM aqueous sodium acetate solution at pH 5. The suspension was incubated at 37 °C for 24 h, followed by 15 min at 90 °C and filtration through a syringe filter (0.2 μm). The filtered solution was stored at -4 °C. The pre-treated cellulose fraction solution contained glucose (39.3±4.7mM) and cellobiose (8.7±2.2 mM) as determined by HPLC. Control experiments with the recovered solid after treatment of white Birch with dioxane/HCl/HCOOH under the same condition in the absence of cellulase did not show any formation of glucose or cellobiose.

CP|MWCNT electrode preparation. A suspension containing MWCNT in ethanol (1.67 mL g⁻¹) and 2 vol% of a 5 wt% Nafion solution was sonicated for 15 minutes. The suspension was then dropcasted on a defined area of carbon paper (0.1 mL cm⁻²) that was masked with Teflon tape followed by overnight drying at room temperature. The electrode was then taped to a metal rod using a copper tape and the metal rod and copper tape was wrapped with Parafilm.

CP|CoPL electrode preparation. A suspension containing MWCNT in DMF (3.16 mg g^{-1}) was sonicated for 10 min, subsequently this ink was diluted 25% by adding 0.4 mM **CoPL** in DMF to achieve $2.37 \text{ mg MWCNT g}^{-1}$ and 0.1 mM **CoPL**. This ink was further sonicated for 10 min and then dropcasted on a defined area (masked with Teflon tape) of carbon paper (0.1 mL cm^{-2}), followed by drying overnight at room temperature. The electrode was then taped to a metal rod using a copper tape and the metal rod and copper tape was wrapped with Parafilm.

Photocatalytic experiments. In a typical experiment, to TiO_2 (P25, 5 mg) was added 2 mL of MeCN and 1 mL of the solution obtained from cellulase pre-treatment in a glass photoreactor (7.74 mL total volume) equipped with a magnetic stir bar. 50 nmol of **CotpyP** (from a freshly prepared 2 mM solution in H_2O ; 0.025 mL) was added, and the photoreactor (3 mL solution with 4.74 mL headspace) was capped with a rubber septum and purged with CO_2 (100 vol% or 20 vol% balanced with N_2) controlled by mass flow controllers for 15 min at 15 mL min^{-1} , followed by stirring for 15 min in the dark. The photoreactor (kept at $25 \text{ }^\circ\text{C}$ and stirred at 600 rpm) was then irradiated with a calibrated solar light simulator (Newport Oriel, 100 mW cm^{-2}) equipped with an air mass 1.5 global (AM 1.5G) filter and a water filter to remove infrared radiation. The photocatalytic process was monitored by analysing the headspace after 6 and 24 h by gas chromatography to monitor H_2 and CO formation. Formate in the solution (diluted in H_2O (1:9 v:v photocatalysis solution: H_2O)) were analysed at the end of the photocatalytic studies (after 24 h) by ion chromatography.

CO_2 -to-CO conversion efficiency. Photocatalytic CO_2 -to-CO conversion efficiency (%) of $\text{TiO}_2/\text{CotpyP}$ was calculated by dividing the mol of CO produced after 24 h by the mol of CO_2 in the photoreactor headspace and multiplying the product by 100. The mol of CO_2 was obtained using the ideal gas law equation ($pV = nRT$), where p is 1 atm, V is the volume of the reactor headspace in L multiplied by the molar fraction of CO_2 , R is the ideal gas constant ($0.082 \text{ atm L mol}^{-1} \text{ K}^{-1}$) and T is 298.15 K.

Isotopic labelling experiments. To a suspension of cellulose (300 mg) in a 50 mM aqueous sodium acetate solution (6 mL) at pH 5 (adjusted by the addition of HCl) at $37 \text{ }^\circ\text{C}$ was added cellulase (15 mg in 1.5 mL) in a 50 mM aqueous sodium acetate solution at pH 5. The suspension was incubated at $37 \text{ }^\circ\text{C}$ for 24 h, followed by 15 min at $90 \text{ }^\circ\text{C}$ and filtration through a syringe filter ($0.2 \text{ }\mu\text{m}$). The filtered solution was stored at $-4 \text{ }^\circ\text{C}$. The pre-treated cellulose solution contained glucose ($53 \pm 2 \text{ mM}$) and cellobiose ($26 \pm 1 \text{ mM}$) as determined by HPLC. To a glass photoreactor vial (7.74 mL total volume) equipped with a magnetic stir bar was added 5 mg of TiO_2 which was suspended in 2.95 mL of 2:1 v:v MeCN:pre-treated cellulose solution. The molecular catalyst **CotpyP** (0.025 mL 50 nmol, 2 mM in H_2O) and 0.025 mL H_2O (to reach 3 mL) was added and the photoreactor was capped with a rubber septum. The photoreactor

was then degassed for one min (vacuum at 10^{-2} mbar) after which $^{13}\text{CO}_2$ (1 bar) was introduced. The photoreactor (kept at $25\text{ }^\circ\text{C}$ and stirred at 600 rpm) was then irradiated (AM 1.5G, 100 mW cm^{-2}). The headspace was then transferred to an air-tight evacuated IR cell (10 cm path length, equipped with KBr windows) and the background (IR cell under vacuum) corrected IR spectrum was recorded to detect ^{12}CO and ^{13}CO .

Flow CO_2 electroreduction. Electrochemical experiments were performed on an Ivium Compactstat electrochemical analyser controlled by the Iviumsoft software. In a typical experiment a 0.1 M NaHCO_3 solution in H_2O was prepared and used for the anolyte and catholyte separated by a Nafion membrane. Chronoamperometry (CA) was performed with CP|CoP_L as working electrode, Pt foil as counter electrode and Ag/AgCl as reference electrode. The electrochemical cell was capped with rubber septa and the catholyte was purged for 30 minutes with N_2 (For screening electrocatalytic performance of different gas composition) or the desired gas composition (For CA at a given gas composition (20 or 100 vol%) for 4h) at a flow rate of 20 mL min^{-1} controlled by mass flow controllers (Brooks) to remove oxygen. Afterwards the flow rate was reduced to 9 mL min^{-1} and a potential of -1.2 V vs. Ag/AgCl was applied. CA was run at -1.2 V vs. Ag/AgCl for 4 h at constant gas flow of 20 or 100 vol% or during screening different gas composition, the electrocatalytic activity was measured for 30 min under N_2 followed by increasing the CO_2 concentration to 10, 20, 50 and 100 vol% every 45 min. Electrochemical experiments were carried out at room temperature. The formed gaseous products (H_2 and CO) were measured by online GC measurement (injection every 4.5 min) using an Agilent 7890A gas chromatograph equipped with an HP-5 molecular sieve column and a thermal conductivity detector using He as the carrier gas. Calibration was performed by determining the response factor by flowing a calibration gas with known CO and H_2 composition under the same condition (9 mL min^{-1}).

Electrocatalytic lignin model substrate & lignin oxidation. Electrochemical experiments were performed on a PalmSens MultiEMStat³⁺ potentiostat. In a typical experiment, 0.1 M Na_2CO_3 solution in MeCN: H_2O (1:1 vol%) was used as the electrolyte. To the electrolyte was added 0.01 M of the lignin model substrate or the lignin fraction from pre-treating 250 mg white birch in Dioxane/ HCl / H_2O . The solution was then used as anolyte (8 mL) in electrocatalysis with 0.1 M Na_2CO_3 solution in MeCN: H_2O (1:1 vol%), and separated from the catholyte by a Selemion anion exchange membrane, and the electrochemical cell was capped with rubber septa. Cyclic voltammetry (CV) or chronoamperometry (CA) were performed with CP|MWCNT as working electrode, Pt foil as counter electrode and Ag/AgCl (sat. KCl) as reference electrode. CV scans were run from -0.2 to 1.0 V vs. Ag/AgCl followed by a backwards scan to -0.2 V vs. Ag/AgCl with a scan rate of 50 mV s^{-1} . CA experiments were performed for 4 h at 1.0 V vs. Ag/AgCl. Electrochemical experiments were carried out at room temperature. To

analyse the products after electrocatalysis, the anolyte was acidified to a pH of 3 with 0.1 M HCl, extracted with EtOAc (3 x 5 mL), dried over MgSO₄, filtered and dried at 40 °C under vacuum to obtain a light brown solid. The solid was further analysed by ¹H NMR in CDCl₃ with mesitylene as internal standard. Control experiments were performed without an applied potential and stirring the anolyte containing the lignin model substrate or lignin fraction for 4 h followed work up and analysis by ¹H NMR in CDCl₃.

Electrocatalytic lignin dimer model & lignin oxidation coupled to CO₂ reduction.

Electrochemical experiments were performed on an Ivium Compactstat electrochemical analyser controlled by the Iviumsoft software. In a typical experiment a 0.1 M Na₂CO₃ solution in MeCN:H₂O (1:1 vol%) was prepared and used for the electrolyte. To the electrolyte was added 0.01 M of the lignin model substrate or the lignin fraction from pre-treating 250 mg white birch in Dioxane/HCl/H₂O. The solution was then used as anolyte (4 mL). A 0.1 M NaHCO₃ solution in H₂O was used as catholyte. The anolyte and catholyte were separated by a bipolar membrane. Electrolysis was performed with CP|MWCNT and CP|CoP_L as anode and cathode, respectively. The electrochemical cell was capped with a rubber septa and the catholyte was purged for 30 minutes with 20 vol% CO₂ (balanced by N₂) at a flow rate of 20 mL min⁻¹ controlled by mass flow controllers (Brooks) to remove oxygen. Afterwards the flow rate was reduced to 9 mL min⁻¹ and a potential of U_{app} = +3 V was applied and run for 4 h. Electrochemical experiments were carried out at room temperature. The formed gaseous products (H₂ and CO) on the cathode side were measured by online GC measurement (injection every 4.25 min) using an Agilent 7890A gas chromatograph equipped with an HP-5 molecular sieve column and a thermal conductivity detector using He as the carrier gas. Calibration was performed by determining the response factor by flowing a calibration gas with known CO and H₂ composition under the same condition (9 mL min⁻¹). To analyse the products, after electrocatalysis the anolyte was acidified to a pH of 3 with 0.1 M HCl, extracted with EtOAc (3 x 5 mL), dried over MgSO₄, filtered and dried at 40°C under vacuum to obtain a light brown solid. The solid was further analysed by ¹H NMR in CDCl₃ with mesitylene as internal standard. Control experiments were performed under the same conditions but without the lignin model substrate or lignin fraction dissolved in the anolyte.

Single-pass CO₂ conversion efficiency. The electrochemical single-pass CO₂ conversion efficiency (%) of CP|CoP_L was calculated by dividing the rate of CO formation (mol min⁻¹) by the flow rate of CO₂ (mol min⁻¹) and multiplying the product by 100. The flow rate of CO₂ was obtained by transforming ml min⁻¹ to mol min⁻¹ using the ideal gas law equation ($pV = nRT$), where p is 1 atm, V is the flow rate of CO₂ in L min⁻¹ (e.g., 1.8 10³ L min⁻¹ for 20vol% CO₂), R is the ideal gas constant (0.082 atm L mol⁻¹ K⁻¹) and T is 298.15 K.

Data analysis. Experiments were performed in triplicates and the results are represented with the mean (\bar{x}) and standard error ($\sigma_{\bar{x}}$) expressed as $\bar{x} \pm \sigma_{\bar{x}}$ with

$$\bar{x} = \frac{1}{n} \sum_{i=1}^n x_i$$
$$\sigma_{\bar{x}} = \sqrt{\frac{1}{(n-1)} \sum_{i=1}^n (x_i - \bar{x})^2}$$

where n is the number of measurements and x_i the individually determined value.

Conflicts of interest

There are no conflicts to declare.

Acknowledgements

We would like to thank the European Research Council (ERC) for a Proof of Concept Grant (SolReGen; to E.L. and E.R), the European commission for a Horizon 2020 Marie Skłodowska-Curie individual Fellowship (GAN 891338, to S.R.J.), the Swiss National Science Foundation (Early Postdoc Fellowship: P2EZP2-191791 to E.L.), the Leverhulme Trust (P80336 to E.L. and E.R.), and the HRH The Prince of Wales Commonwealth Scholarship (Cambridge Trust; to S.B.). The authors also thank Dr. Nigel Howard at the University of Cambridge for performing elemental and ICP-OES analyses, and Dr. Heather Greer at the University of Cambridge for assistance with the electron microscopy, as well as Dr. Tessel Bouwens, Dr. Bidyut B. Sarma and Dr. Yongpeng Liu for useful feedback on the manuscript.

References

1. S. C. Peter, *ACS Energy Lett.*, 2018, **3**, 1557-1561.
2. G. W. Huber, S. Iborra and A. Corma, *Chem. Rev.*, 2006, **106**, 4044-4098.
3. R. Schlögl, *Green Chem.*, 2021, **23**, 1584-1593.
4. W. Schutyser, T. Renders, S. Van den Bosch, S. F. Koelewijn, G. T. Beckham and B. F. Sels, *Chem. Soc. Rev.*, 2018, **47**, 852-908.
5. X. Liu, X. Duan, W. Wei, S. Wang and B.-J. Ni, *Green Chem.*, 2019, **21**, 4266-4289.
6. *TAPPI T 222 om-02*, 2006.
7. L. Shuai, M. T. Amiri, Y. M. Questell-Santiago, F. Héroguel, Y. Li, H. Kim, R. Meilan, C. Chapple, J. Ralph and J. S. Luterbacher, *Science*, 2016, **354**, 329-333.
8. M. M. Abu-Omar, K. Barta, G. T. Beckham, J. S. Luterbacher, J. Ralph, R. Rinaldi, Y. Román-Leshkov, J. S. M. Samec, B. F. Sels and F. Wang, *Energy Environ. Sci.*, 2021, **14**, 262-292.
9. C. Zhang and F. Wang, *Acc. Chem. Res.*, 2020, **53**, 470-484.

10. Z. Sun, B. Fridrich, A. de Santi, S. Elangovan and K. Barta, *Chem. Rev.*, 2018, **118**, 614-678.
11. M. Rafiee, M. Alherech, S. D. Karlen and S. S. Stahl, *J. Am. Chem. Soc.*, 2019, **141**, 15266-15276.
12. A. M. Appel, J. E. Bercaw, A. B. Bocarsly, H. Dobbek, D. L. DuBois, M. Dupuis, J. G. Ferry, E. Fujita, R. Hille, P. J. A. Kenis, C. A. Kerfeld, R. H. Morris, C. H. F. Peden, A. R. Portis, S. W. Ragsdale, T. B. Rauchfuss, J. N. H. Reek, L. C. Seefeldt, R. K. Thauer and G. L. Waldrop, *Chem. Rev.*, 2013, **113**, 6621-6658.
13. A. C. Forse and P. J. Milner, *Chemical Science*, 2021, **12**, 508-516.
14. S. E. Renfrew, D. E. Starr and P. Strasser, *ACS Catal.*, 2020, **10**, 13058-13074.
15. E. Pérez-Gallent, C. Vankani, C. Sánchez-Martínez, A. Anastasopol and E. Goetheer, *Ind. Eng. Chem. Res.*, 2021, **60**, 4269-4278.
16. T. Nakajima, Y. Tamaki, K. Ueno, E. Kato, T. Nishikawa, K. Ohkubo, Y. Yamazaki, T. Morimoto and O. Ishitani, *J. Am. Chem. Soc.*, 2016, **138**, 13818-13821.
17. G. Lee, Y. C. Li, J.-Y. Kim, T. Peng, D.-H. Nam, A. Sedighian Rasouli, F. Li, M. Luo, A. H. Ip, Y.-C. Joo and E. H. Sargent, *Nat. Energy*, 2021, **6**, 46-53.
18. A. Khurram, M. He and B. M. Gallant, *Joule*, 2018, **2**, 2649-2666.
19. A. Khurram, L. Yan, Y. Yin, L. Zhao and B. M. Gallant, *J. Phys. Chem. C*, 2019, **123**, 18222-18231.
20. S. Kar, M. Rahaman, V. Andrei, S. Bhattacharjee, S. Roy and E. Reisner, *Joule*, 2023, **7**, 1496-1514.
21. A. Perazio, G. Lowe, R. Gobetto, J. Bonin and M. Robert, *Coord. Chem. Rev.*, 2021, **443**, 214018.
22. H. Kumagai, T. Nishikawa, H. Koizumi, T. Yatsu, G. Sahara, Y. Yamazaki, Y. Tamaki and O. Ishitani, *Chemical Science*, 2019, **10**, 1597-1606.
23. X. Du, H. Zhang, K. P. Sullivan, P. Gogoi and Y. Deng, *ChemSusChem*, 2020, **13**, 4318-4343.
24. C. Yang, S. Maldonado and C. R. J. Stephenson, *ACS Catal.*, 2021, **11**, 10104-10114.
25. D. T. Whipple and P. J. A. Kenis, *J. Phys. Chem. Lett.*, 2010, **1**, 3451-3458.
26. M. F. Kuehnel and E. Reisner, *Angew. Chem. Int. Ed.*, 2018, **57**, 3290-3296.
27. A. V. Puga, *Coord. Chem. Rev.*, 2016, **315**, 1-66.
28. S. Bhattacharjee, M. Rahaman, V. Andrei, M. Miller, S. Rodríguez-Jiménez, E. Lam, C. Pornrungrroj and E. Reisner, *Nat. Synth.*, 2023, **2**, 182-192.
29. E. Lam and E. Reisner, *Angew. Chem. Int. Ed.*, 2021, **60**, 23306-23312.
30. A. K. Sinha, U. K. Sharma and N. Sharma, *Int. J. Food Sci. Nutr.*, 2008, **59**, 299-326.
31. T. Kawai and T. Sakata, *Nature*, 1980, **286**, 474-476.
32. J. C. Colmenares, A. Magdziarz and A. Bielejewska, *Bioresour. Technol.*, 2011, **102**, 11254-11257.
33. L. Da Vià, C. Recchi, E. O. Gonzalez-Yañez, T. E. Davies and J. A. Lopez-Sanchez, *Appl. Catal. B: Environ.*, 2017, **202**, 281-288.
34. N. Elgrishi, M. B. Chambers and M. Fontecave, *Chem. Sci.*, 2015, **6**, 2522-2531.
35. J. J. Leung, J. Warnan, K. H. Ly, N. Heidary, D. H. Nam, M. F. Kuehnel and E. Reisner, *Nat. Catal.*, 2019, **2**, 354-365.
36. S. Rodríguez-Jiménez, H. Song, E. Lam, D. Wright, A. Pannwitz, S. A. Bonke, J. J. Baumberg, S. Bonnet, L. Hammarström and E. Reisner, *J. Am. Chem. Soc.*, 2022, **144**, 9399-9412.
37. C. D. Sahm, G. M. Ucoski, S. Roy and E. Reisner, *ACS Catal.*, 2021, **11**, 11266-11277.
38. C. P. O'Brien, R. K. Miao, S. Liu, Y. Xu, G. Lee, A. Robb, J. E. Huang, K. Xie, K. Bertens, C. M. Gabardo, J. P. Edwards, C.-T. Dinh, E. H. Sargent and D. Sinton, *ACS Energy Letters*, 2021, **6**, 2952-2959.
39. M. Fache, B. Boutevin and S. Caillol, *ACS Sustain. Chem. Eng.*, 2016, **4**, 35-46.
40. M. Liu, Y. Wen, J. Qi, S. Zhang and G. Li, *ChemistrySelect*, 2017, **2**, 4956-4962.
41. P. Parpot, A. P. Bettencourt, A. M. Carvalho and E. M. Belgsir, *J. Appl. Electrochem.*, 2000, **30**, 727-731.

42. C. Lan, H. Fan, Y. Shang, D. Shen and G. Li, *Sustain. Energy Fuels*, 2020, **4**, 1828-1836.
43. J. King and S. S. C. Chuang, *Catal. Commun.*, 2021, **149**, 106219.
44. D. Wang, S. H. Lee, S. Han, J. Kim, N. V. T. Trang, K. Kim, E.-G. Choi, P. Boonmongkolras, Y. W. Lee, B. Shin, Y. H. Kim and C. B. Park, *Green Chem.*, 2020, **22**, 5151-5160.
45. D. M. Alonso, S. H. Hakim, S. Zhou, W. Won, O. Hosseinaei, J. Tao, V. Garcia-Negron, A. H. Motagamwala, M. A. Mellmer, K. Huang, C. J. Houtman, N. Labbé, D. P. Harper, C. T. Maravelias, T. Runge and J. A. Dumesic, *Sci. Adv.*, 2017, **3**, e1603301.
46. E. Cooreman, T. Vangeel, K. Van Aelst, J. Van Aelst, J. Lauwaert, J. W. Thybaut, S. Van den Bosch and B. F. Sels, *Ind. Eng. Chem. Res.*, 2020, **59**, 17035-17045.
47. H. Ababneh, A. AlNouss and S. A. Al-Muhtaseb, *Processes*, 2022, **10**, 2406.
48. C. Song, W. Pan, S. T. Srimat, J. Zheng, Y. Li, Y.-H. Wang, B.-Q. Xu and Q.-M. Zhu, in *Studies in Surface Science and Catalysis*, eds. S.-E. Park, J.-S. Chang and K.-W. Lee, Elsevier, 2004, vol. 153, pp. 315-322.
49. H. A. Ruiz, M. Conrad, S.-N. Sun, A. Sanchez, G. J. M. Rocha, A. Romani, E. Castro, A. Torres, R. M. Rodríguez-Jasso, L. P. Andrade, I. Smirnova, R.-C. Sun and A. S. Meyer, *Bioresour. Technol.*, 2020, **299**, 122685.
50. H. Nishiyama, T. Yamada, M. Nakabayashi, Y. Maehara, M. Yamaguchi, Y. Kuromiya, Y. Nagatsuma, H. Tokudome, S. Akiyama, T. Watanabe, R. Narushima, S. Okunaka, N. Shibata, T. Takata, T. Hisatomi and K. Domen, *Nature*, 2021, **598**, 304-307.
51. A. Caravaca, W. E. Garcia-Lorefice, S. Gil, A. de Lucas-Consuegra and P. Vernoux, *Electrochemistry Communications*, 2019, **100**, 43-47.
52. X. Ma, J. Albertsma, D. Gabriels, R. Horst, S. Polat, C. Snoeks, F. Kapteijn, H. B. Eral, D. A. Vermaas, B. Mei, S. de Beer and M. A. van der Veen, *Chem. Soc. Rev.*, 2023, **52**, 3741-3777.
53. M. Peer, S. Mehdi Kamali, M. Mahdeyarfar and T. Mohammadi, *Chem. Eng. Technol.*, 2007, **30**, 1418-1425.
54. P. Wattanaphan, T. Sema, R. Idem, Z. Liang and P. Tontiwachwuthikul, *Int. J. Greenh. Gas Control*, 2013, **19**, 340-349.

Table of content:

